BioNN: Bio-Mimetic Neural Networks on Hardware Using Nonlinear Multi-Timescale Mixed-Feedback Control for Neuromodulatory Bursting Rhythms

Kangni Liu, *Student Member, IEEE*, Shahin Hashemkhani, *Student Member, IEEE*, Jonathan Rubin, *Member, IEEE*, and Rajkumar Kubendran, *Senior Member, IEEE*

***Abstract*— Biological neurons exhibit rich and complex nonlinear dynamics, which are computationally expensive and area/power hungry for hardware implementation. This paper presents a mathematical analysis and hardware realization of neural networks using a nonlinear neuron model that utilizes two excitable systems operating at different timescales. The neuron consists of a mixed-feedback system operating at multiple timescales to exhibit a variety of modalities that resemble the biophysical mechanisms found in neurophysiology. The single neuron dynamics emerge from four voltage-controlled current sources and feature spiking and bursting output modes that can be controlled using tunable parameters. The bifurcation structures of the neuron, modeled as a 4D dynamical system, illustrate the roles of sources acting on different timescales in shaping neural dynamics. A comprehensive understanding of the system's dynamic behavior is obtained by studying the state space variables and performing bifurcation analysis on the different parameters. The model is implemented to a 1mm x 2mm prototype chip utilizing the 180nm CMOS process. Each neural network consists of 1 isolated test neuron and 5 fully connected neurons using 20 synapses. By carefully selecting bias voltages according to the I-V characterization curves, the neurons are shown to exhibit spike, burst, and burst excitable behavior. Multiple small-scale neural networks with inhibitory or excitatory synapses were verified to achieve coupled rhythms with neuron bursts in-phase or out-of-phase. To demonstrate an application, the generated burst waveforms from the 4-neuron network were used to form a Central Pattern Generator (CPG) for locomotion control of the four legs of the Petoi, a quadruped robot, enabling the bot to jump successfully.**

***Index Terms*— Neuromorphic, bio-inspired, nonlinear dynamics, mixed-feedback control, coupled neural networks.**

I. Introduction

ARTIFICIAL Neural Networks (ANNs), and their capability to address complex tasks with high efficiency have attracted remarkable interest for more than a decade [1]. Neuron models used in ANNs are highly simplified in function and operation, to facilitate scaling to large networks. The most popular implementation that is widely adopted in modern AI hardware is the Rectified Linear Unit (ReLU) [2], [3]. The ReLU neuron primarily realizes a linear activation function for all positive inputs, while rectifying negative inputs to zero, thus introducing a simple form of nonlinearity, as shown in Fig.1. Such a simplified model was sufficient to train large networks with the backpropagation algorithm and yield exceptional accuracy, though it is not a bio-mimetic neuron model since it does not generate 'spikes' and neglects the highly nonlinear nature of neurons and their temporal dynamics. On the other hand, Neuromorphic Spiking Neural Networks (SNNs) [4], [5], which intend to be bio-inspired, use a Leaky Integrate-and-Fire (LIF) neuron that can generate voltage spikes or 'events' similar to biological neurons. The LIF neuron is implemented using an RC network that linearly integrates an applied external current to produce a voltage ramp [6], [7], [8], [9]. The LIF generates a spike once the ramp input exceeds a predefined threshold, after each integration cycle. Thus, the LIF neuron realizes the step activation, which is also a simple form of nonlinearity generating 'all-or-nothing' events as voltage spikes. SNN mimics biology better than ANN, however, still fails to capture the temporal dynamics of biological neurons to exhibit more complex behavior such as burst generation. Though ReLU and LIF neurons have been extremely successful when used in a predominantly feed-forward network, they are not suitable to demonstrate neuroscientific principles such as multiple modes of operation (spiking, bursting, etc), coupled oscillations with excitatory and inhibitory connections controlled through a single parameter: external applied current (I_{app}), and bursting rhythm generation with neurons in-phase or out-of-phase.

Biological neurons exhibit rich nonlinear dynamics both at the single neuron level and at the network level, which is enabled through neuromodulation, using multiple feedback paths (local and global) operating at multiple timescales [11], [12]. Complex neuron models inspired by neurophysiology have been proposed before, like the Hodgkin-Huxley model [13] and the Izhikevich model [14]. These models capture the biophysics of the neuron accurately but are based on non-intuitive computationally expensive differential equations

Manuscript received 31 May 2023; revised 26 September 2023; accepted 23 October 2023. Date of publication 3 November 2023; date of current version 29 December 2023. This article was recommended by Guest Editor J. Eshraghian. *(Kangni Liu and Shahin Hashemkhani contributed equally to this work.) (Corresponding author: Kangni Liu.)*

Kangni Liu, Shahin Hashemkhani, and Rajkumar Kubendran are with the Department of Electrical and Computer Engineering (ECE), University of Pittsburgh, Pittsburgh, PA 15261 USA (e-mail: connie.liu@pitt.edu; shh199@pitt.edu; rajkumar.ece@pitt.edu).

Jonathan Rubin is with the Department of Mathematics, University of Pittsburgh, Pittsburgh, PA 15260 USA (e-mail: jonrubin@pitt.edu).

Color versions of one or more figures in this article are available at https://doi.org/10.1109/JETCAS.2023.3330084.

Digital Object Identifier 10.1109/JETCAS.2023.3330084

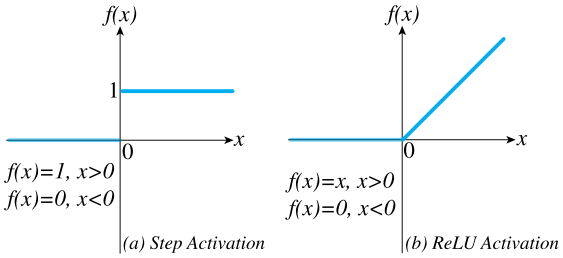

Fig. 1. Neuron activation functions for (a) Spiking Neural Networks (Step) and (b) Artificial Neural Networks (ReLU).

that are hard to implement on hardware with minimal circuit elements. Previous work has shown that neuromodulation of a single neuron can be efficiently implemented using a nonlinear circuit model with mixed feedback paths (positive and negative), operating at different timescales [15]. Realizing this dynamic neuron model on hardware could result in the development of Bio-mimetic Neural Networks (BioNN). A critical application of BioNN is the demonstration of a potential implementation of the Central Pattern Generator (CPG) network that can generate rhythms consistent with those believed to underlie mammalian locomotion [16].

CPGs are highly optimized neural circuits found in the nervous systems of animals, responsible for generating rhythmic and coordinated patterns of activity to enable movement such as walking, swimming, or flying. These specialized networks exhibit a remarkable ability to produce rhythmic behaviors without requiring continuous sensory input or higher-level control. CPGs are often located in the spinal cord or other central nervous system regions and consist of interconnected neurons that communicate through intricate synaptic connections. The coordinated firing of these neurons generates a repetitive and robust pattern of activity, allowing animals to engage in rhythmic motions essential for their survival and locomotion. CPGs not only provide insight into the fundamental principles of neural circuitry but also serve as a source of inspiration for the development of bio-inspired robotics and control systems [17], [18], [19], [20], [21], [22], [23], with potential applications in fields ranging from healthcare to autonomous vehicles. Efforts have been made to utilize a more bio-inspired neuron model such as the Hudgin-Huxley (HH) model [13], and the Izhikevich (IZ) model [14]. The HH model and related variants based on the HH formalism provide the most complete modeling framework typically used to represent biological neurons, while the (IZ) model is a mathematically simplified version that captures the dynamic of its biological counterpart but not necessarily in a bio-physically meaningful manner [11]. Both suffer from poor compatibility with hardware implementations given the complexity of their describing equations which is intensely computationally expensive. According to the biophysics of neuron cells, neuron operation can be described as a non-linear dynamical system with multiple feedback loops working in different time scales [12], [24], [25]. Inspired by such elegant architecture, Ribar and Sepulchre [10], [15] introduce a novel model that sufficiently captures the temporal dynamics of biological neurons, resulting in tonic spiking, and tonic bursting [24], and is hardware-friendly. This bio-mimetic neuron model can be controlled at single neuron level or network level through modulation of a single parameter: the external applied current (I_{app}). Such an approach could potentially bridge the gap between complexity and hardware feasibility and pave the way for further improvement in this field.

This paper is an extension of our previous work presented at the ISCAS conference [26], with significant improvements such as an upgraded chip design, additional analysis and measured results of several neural networks including a demonstration of the CPG network for robot locomotion control. This paper presents a mathematical analysis and Application Specific Integrated Circuit (ASIC) implementation of the nonlinear neuron model proposed in [15]. Section II presents a concise overview of the nonlinear neuron model. Section III presents the bifurcation study of the nonlinear dynamical system of equations and its implications in understanding how to tune the proposed neuron model. Section IV illustrates the chip architecture of the neural network circuit design. Section V reviews the measured result of the prototype chip at both the single neuron level and network level, including a robot control application. Section VI provides a detailed discussion to explain about the significance of the contributions of this work by comparing with other state-of-the-art biophysical neuron models (neurons that can produce bursting behavior) in the literature. This section also mentions our planned future work in this direction. Section VII provides a comprehensive summary of our work, concluding the paper.

II. Background

The neuron plays a pivotal role as one of the two primary components within both biological neural circuits and ANNs. Remarkable advancements in machine learning algorithms have often overshadowed the importance of revisiting the neuron's fundamental characteristics. Consequently, the majority of research articles tend to concentrate on algorithms to improve network efficiency. While this focus was adequate in the past, the ubiquity of AI-based devices in our daily lives and the pressing issue of excessive resource and power consumption highlight the need for an innovative neuron model that closely emulates biological counterparts, especially in edge computing applications.

Numerous distinct neuron models have been proposed, each offering its unique set of advantages and disadvantages. However, these models generally prioritize different levels of biological realism while overlooking the complexities of hardware implementation. Izhikevich, for example, categorized various neuron models based on their dynamic behaviors and degrees of biological fidelity [11]. Implementing these neuron models in hardware is feasible, provided sufficient resources are available. Nevertheless, when it comes to dedicated applications and ASIC design, selecting an appropriate model that accurately represents neuron dynamics and is easy to implement becomes a formidable challenge. Moreover, if the underlying equations governing the neuron model are overly complex, scaling up the size of neural networks, particularly using conventional digital design approaches, becomes exceedingly complicated and resource-intensive. A potential solution lies in rigorously assessing the application's requirements

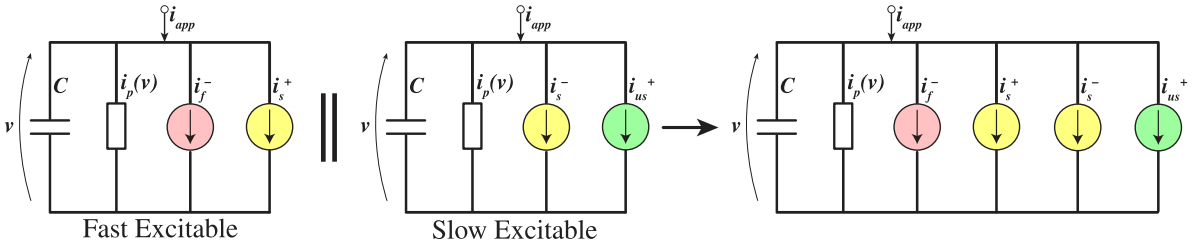

Fig. 2. Construction of the bio-mimetic neuron model by combining two excitable systems working at different timescales. An excitable membrane modeled as a highly parallel circuit, including a passive RC network and four voltage-gated conductance channels inspired by the Na+/K+ ion channels found in neurophysiology. Each color represents a different timescale [10]. The fast (pink) negative conductance (i_f^-) operates in microsecond (μs) range, the slow (yellow) positive (i_s^+) and slow (yellow) negative (i_s^-) conductances in millisecond (ms) and ultra-slow (green) positive conductance (i_{us}^+) in 100ms range.

and identifying the essential dynamic behaviors of neurons. Subsequently, optimizing the design methodology becomes imperative to achieve a hardware-friendly realization.

One promising neuron model, proposed in a study by Ribar et al. [15] and closely resembling the physiological neuromodulation of a single neuron, offers not only ease of hardware implementation but also great potential at network scale modulation. Drawing inspiration from the biophysics of actual neuron cells, this model comprises multiple gated current sources operating at different time scales, akin to the ion channels found in cell membranes. This neuron model is constructed by interconnecting an excitable system, which will be comprehensively described in the subsequent sections.

The schematic of the neuron model is illustrated in Fig. 2. This neuron model comprises the interconnection of two excitable systems operating at different time scales. Each excitable system is composed of two voltage-controlled current sources (VCCS) and a passive circuit with a Resistor-Capacitor (RC) configuration. By connecting these two excitable systems in parallel, we establish a common equivalent passive system between them. The relationship between current and voltage in each VCCS is $I_x = f(V_x) = Tanh(v_x)$ where x indicates the internal time scale of the excitable system. The VCCS will be realized using a straightforward Operational Transconductance Amplifier (OTA), where the design methodology will be presented in the upcoming section.

The neuron model, as illustrated in Fig. 2, has the capability to generate tonic spiking and bursting [27], which are essential for realizing a CPG applicable in robotics and locomotion. Furthermore, once the neuron parameters are initially configured, the operational mode can be seamlessly switched between spiking and bursting solely by adjusting the applied current I_{app}, mimicking the behavior of actual neurons. These distinctive characteristics make this model a promising solution for a wide range of applications.

III. Bifurcation Analysis

Studying dynamical systems involves comprehending the equilibrium points and ways in which their existence and stability change as system parameters are varied, which are commonly referred to as bifurcations. Bifurcation is a concept that is widely used in various fields, including mathematics, physics, biology, and engineering. It refers to the process or occurrence of a system undergoing an abrupt change in behavior as a result of a small, gradual change in its parameters. The current section is dedicated to providing a summary of the analysis method that has been used in this paper to analyze the dynamical system. Initially, an overview of the excitable system and its complete study will be presented then the section will be completed by providing the analysis of the full neuron model.

A. Neuron Excitable Behavior

According to Sepulchre et al, excitability is the ability of a system to respond to pulse inputs in an all-or-none manner. Given a system in an equilibrium state, a small input perturbation causes a small output change, however, amplifying the perturbation beyond a certain limit leads to large output variation [28]. Such behavior is primarily observed in neurons, where membrane voltage generates an action potential in response to sufficient current flow within neurons [29]. This system can be decomposed into three distinct elements: a passive circuit, a switch, and a regulator. A monotonic $(I-V)$ curve accounts for the passive behavior, a switch accounts for localized temporal dynamical behavior, and a regulator provide a temporal control method to achieve the refractory method.

To have a system capable of showing the dynamical behavior of interest, one positive and one negative feedback with variable gains and opposite signs that are working in different time scales are necessary. Depending on which feedback loop dominates the other locally, the static I-V characteristic curve of the system can be monotonic or hysteretic. Reference [28]it is intuitive to understand the reason for such a requirement. Positive feedback by its nature is a reinforcement factor that amplifies the sampled output by a gain and adds this to the input. Such a condition in the electronic system results in the saturation of the system output to the maximum available output. To prevent such an occurrence a counter-force, negative feedback, is necessary to release the system from saturation. Having two competing forces is necessary but not sufficient to generate complex dynamical behavior as long as they are working on the same time scale. By introducing different time constants for positive and negative feedback gain, the system can show various local temporal behaviors according to the relative strength of feedback loops.

Multiple realization methods exist for an excitable system, each capable of capturing different ranges of physiological neuron behaviors. Various form of bursting and their mechanism are studied here [30]. Our method prioritizes simplicity in hardware implementation while demonstrating two prominent types of neuron behavior: tonic spiking and tonic bursting. The advantage of the excitable system as shown in Fig. 2(Left),

is being hardware friendly and expandability by simply paralleling a single block to generate more complex behavior that will be discussed in the neuron model section. Considering all the requirements, the model in Fig. 2 (Left) [10] is being used.

$$\begin{aligned} C\dot{V_m} &= -(I_p^+(V_m) + I_f^-(V_f) + I_s^+(V_s) - I_{app}) \\ \tau_f \dot{V_f} &= V_m - V_f \\ \tau_s \dot{V_s} &= V_m - V_s \\ &\times (\epsilon = \frac{\tau_f}{\tau_s} \ll 1) \end{aligned} \tag{1}$$

where the I_p^+ is a monotonic passive element with a positive slope, $I_x^{\pm} = \alpha_x^{\pm} \tanh(V_x - \delta_x^{\pm})$ is VCCS to realize the switch and regulate components, where the subscript represents the time scale ($x = f$) for fast and ($x = s$) for slow and superscript indicate the sign of the gain. Finally, I_{app} is an external current injected into the system. Given the complexity involved in analyzing the excitable system due to its nonlinear nature, the study of the problem has been simplified by isolating one parameter at a time and investigating its effect.

B. Analysis Methods

The proposed excitable system according to Eq.1 and subsequent equation of the complete neuron model comprise an autonomous system of ordinary differential equations (ODEs). An autonomous system of ordinary differential equations (ODEs) refers to a set of equations that describe the behavior of a dynamical system without explicit dependence on time. In such systems, the rates of change of the variables are solely determined by the current state of the system itself, rather than being influenced by an external time parameter. This characteristic gives autonomous ODE systems a self-contained nature, where the evolution of the variables is solely governed by the interplay between their current values. To analyze the autonomous system of ordinary differential equation (ODE) the following steps are followed:

1) Reduce the dimension of the system given the time-scale separation
2) Find equilibrium points (EQP) and nullclines(NC) of systems
3) Linear approximate system in the neighborhood of the EQP
4) calculation of eigenvalue and classifying the EQP type based on Poincare's diagram
5) Estimate the behavior of the system given its linearized phase portraits following the Hartman-Grobman theorem [31].

To simplify the mathematical solution without loss of generality, we set $\delta_x^{\pm} = 0$ and $-|\alpha_f^-| = |\alpha_s^+| = \alpha(\alpha > 0)$, $C = 1$ and $\epsilon = 0.02$. It is worth noting that the shape of the curve in a bifurcation diagram will vary depending on different parameter values and will not remain linear. Given adequate time-scale separation, $\epsilon \ll 1$ and having sufficiently small τ_f the fast subsystem follows the membrane voltage instantaneously, therefore, the system can be simplified to a well-known 2D system of ODE as follows:

$$F(V_m, V_s) \triangleq$$

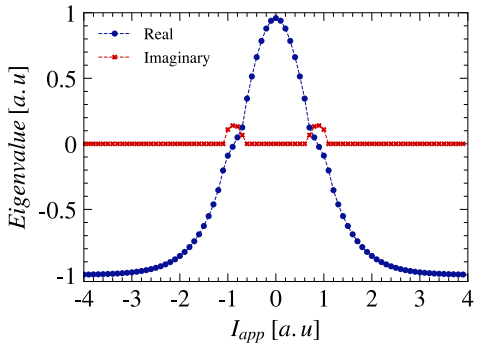

Fig. 3. Eigenvalues of the Jacobian matrix of a linearized system vs. I_{app}. $-|\alpha_f| = |\alpha_s| = 2$, $|\delta_f| = |\delta_s| = 0$, $\epsilon = 0.02$. (a.u stands for arbitrary unit).

$$\begin{aligned} \dot{V_m} &= -(V_m - \alpha \tanh(V_m) + \alpha \tanh(V_s) - I_{app}) \\ G(V_m, V_s) &\triangleq T_s \dot{V_s} = V_m - V_s \end{aligned} \tag{2}$$

The nullclines of a 2D system is calculated by ($\dot{V_m} = 0$) and ($\dot{V_s} = 0$):

$$\begin{aligned} V_m - \alpha \tanh(V_m) &= -\alpha \tanh(V_s) + I_{app} \\ V_m &= V_s \end{aligned} \tag{3}$$

The equilibrium points, the intersection of the two nullclines, given the previous assumption, will be $(V_s, V_m) = (I_{app}, I_{app})$. A common approach to analyzing a system with a complex nonlinear function is to perform a linearization in the vicinity of an EQP and study the behavior of the linearized system. The linearized system is derived by forming the matrix of partial derivatives of the nonlinear equations with respect to the variables and evaluating them at the EQP, also known as the Jacobian Matrix. Although the linearization introduces some approximation error, it allows us to gain insights into the system's stability, controllability, and observability, which are essential for designing control strategies and understanding its overall behavior. The approximated system behavior can be extended to its original non-linear counterpart as long as all eigenvalues have a nonzero real part according to the Hartman-Grobman theorem. [31] The Jacobian matrix of the Eq.2 will be:

$$\begin{aligned} J &= \begin{bmatrix} \frac{\partial F}{\partial V_m} & \frac{\partial F}{\partial V_s} \\ \frac{\partial G}{\partial V_m} & \frac{\partial G}{\partial V_s} \end{bmatrix} \\ &= \begin{bmatrix} \frac{-1+\alpha(1-\tanh^2(V_m))}{C} & \frac{-\alpha(1-\tanh^2(V_s))}{C} \\ \frac{1}{T_s} & \frac{-1}{T_s} \end{bmatrix} \end{aligned} \tag{4}$$

The eigenvalues of the Eq.4 are used to study and categorize the behavior of the EQP given the Poincare classification of an autonomous system. Fig. 3 illustrates the eigenvalues for different EQP given various I_{app}. In addition, Fig. 4 emphasizes the (I_{app}) bifurcation diagram given the different results of eigenvalues, where the red indicates the periodic solution for a given I_{app} and the blue illustrates the stable solution. At the boundary of the transiting from the stable EQP to the periodic solution a Hopf bifurcation is happening. When a dynamical system undergoes a Hopf bifurcation, it transitions from a stable equilibrium state to a limit cycle, giving rise to sustained oscillations.

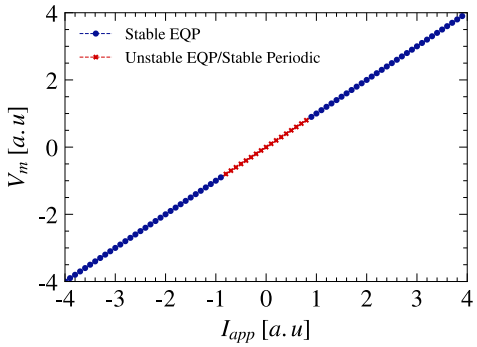

Fig. 4. Bifurcation diagram of an excitable system Eq.5 vs. I_{app}. $-|\alpha_f| = |\alpha_s| = 2$, $|\delta_f| = |\delta_s| = 0$, $\epsilon = 0.02$.

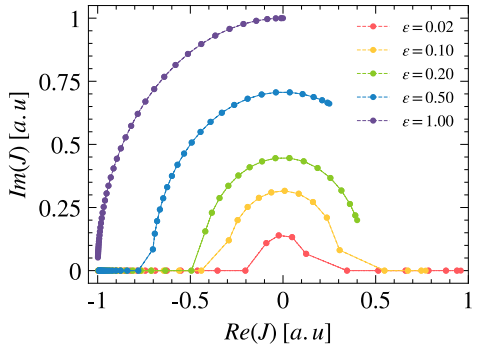

Fig. 5. Effect of time scale separation (ϵ) on Jacobian matrix in complex plane for different I_{app}. Each point indicates different I_{app}. $-|\alpha_f| = |\alpha_s| = 2$, $|\delta_f| = |\delta_s| = 0$.

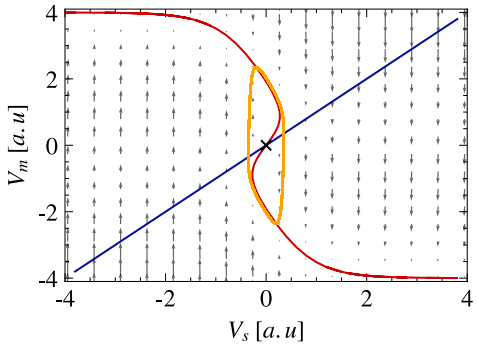

Fig. 6. Phase portrait and trajectory of the solution in vector-field coordinates. $-|\alpha_f| = |\alpha_s| = 2$, $|\delta_f| = |\delta_s| = 0$ and $I_{app} = 0$, $\epsilon = 0.02$.

Furthermore, Fig. 5 highlights the significance of the time-scale separation. As ϵ increases, all the eigenvalues will be located on the left-hand side (LHS) of the complex plane where all the real parts are negative, meaning the stable EQP of the dynamical system and eliminated the possibility of having unstable EQP which is necessary for excitable behavior.

Finally, a solution of the system (orange) together with phase portrait (red and blue) is shown in the vector field of the system in Fig. 6 and its steady state behavior in Fig. 7.

The study will not be complete unless the effect of parameters on the global behavior of a system, such as amplitude and frequency is addressed. Many ways could be opted to describe the relation between amplitude and frequency. Here a potential explanation is provided in a qualitative manner since it makes understanding the underlying operation easier. Fig. 8 includes three trajectories given different parameters. The black trace, a base solution with previously mentioned parameters, and the red and blue traces with different values

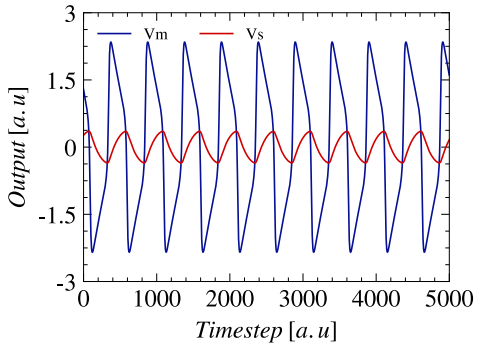

Fig. 7. The steady state voltage response of the fast and slow elements. $-|\alpha_f| = |\alpha_s| = 2$, $|\delta_f| = |\delta_s| = 0$, $I_{app} = 0$ and $\epsilon = 0.02$.

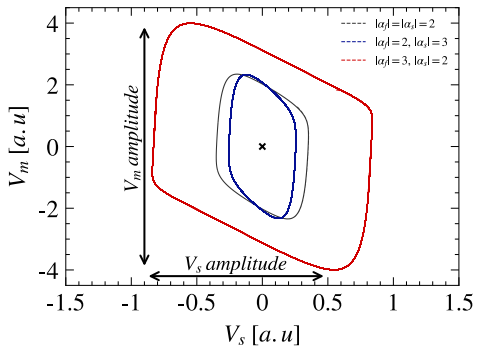

Fig. 8. Effect of $|\alpha_f|$ and $|\alpha_s|$ on the trajectories and overall transient behavior of the system. $|\alpha_f| = |\alpha_s| = 2$ (black), $|\alpha_f| = 3$, $|\alpha_s| = 2$ (red) and $|\alpha_f| = 2$ $|\alpha_s| = 3$ (blue). In all scenarios $|\delta_f| = |\delta_s| = 0$, $I_{app} = 0$ and $\epsilon = 0.02$. The result highlights that the fast element gain controls the amplitude of the membrane (V_m) while the slow element gain modulates the frequency by shrinking the (V_s) travel.

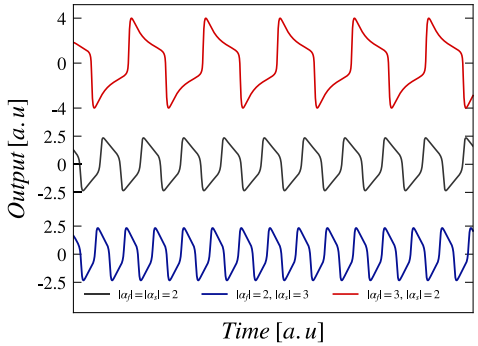

Fig. 9. Neuron membrane voltage V_m for different values of $|\alpha_f|$ *and* $|\alpha_s|$. In all scenarios $|\delta_f| = |\delta_s| = 0$, $I_{app} = 0$ and $\epsilon = 0.02$.

for α_f^- and α_s^+ respectively. The fast element gain acts as a stretch operator that tends to keep the aspect ratio of the trajectory the same. Since both V_m and V_s feel the effect relatively with the same strength, the fast element can be used for tuning both the amplitude and frequency at the same time, while the slow element gain it has a negligible effect on V_m axis and predominantly shrink the maximum swing of V_s. The smaller the swing the faster it can be reached therefore the slow element gain can be considered as a controlling agent of the frequency with negligible effect on amplitude. Fig. 9 illustrates the steady state behavior of membrane voltage according to the Fig. 8 parameters.

C. Neuron Model Analysis

A 2D excitable system (V_m, V_s) similar the one introduced in Eq.1, is incapable of bursting. Bursting is a transition

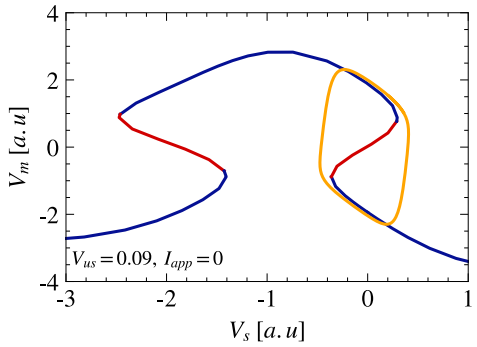

Fig. 10. Bifurcation structure for the fast (V_m, V_f) subsystem with V_s treated as a bifurcation parameter.

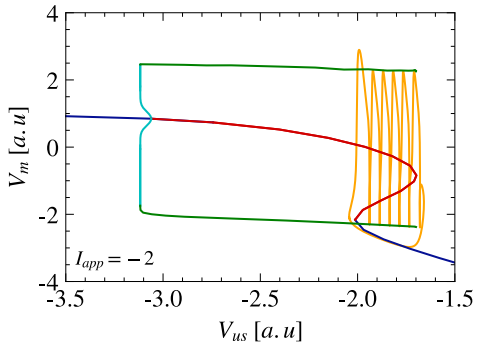

Fig. 11. Bifurcation structure for the (V_m, V_f, V_s) system with V_{us} taken as the bifurcation parameter. The family of unstable periodic orbits is born in a Hopf bifurcation near $V_{us} = -3.2$ and terminates in a homoclinic bifurcation near $V_{us} = -1.7$.

between spiking and resting potential that is repeated over time. According to Izhikevich, the bursting is caused by the modulation of a fast subsystem by a slow variable [30]. To address this issue, another excitable system that is working on a slower time scale can be introduced. The first excitable system, which is responsible for the spike generation is called fast excitable with (τ_f^- and τ_s^+) as its time scale parameters, and the new one is called the slow excitable with (τ_s^- and τ_{us}^+) timescale parameters. The slow excitable system should follow a slower time scale so that it does not interfere with the spike generation but is adequate to cause a transition between periodic spiking dynamics and resting dynamics, to generate a bursting behavior. The system is formed by coupling the fast excitable and slow excitable systems together to satisfy the requirement for a neuron model capable of showing burst and spiking behavior [10], [15]. The final neuron model is shown in Fig. 2 and its governing system of equations, is presented in Eq.5.

$$\begin{aligned} C\dot{V_m} &= -(I_p^+(V_m) + I_f^-(V_f) + I_s^+(V_s) + I_s^-(V_s) \\ &\quad + I_{us}^+(V_{us}) - I_{app}) \\ \tau_f \dot{V_f} &= V_m - V_f \\ \tau_s \dot{V_s} &= V_m - V_s \\ \tau_{us} \dot{V_{us}} &= V_m - V_{us} \\ &\quad \times (\tau_f \ll \tau_s \ll \tau_{us}) \end{aligned} \tag{5}$$

Given the timescale separation, the dimension of the system can be reduced to a 3D system, by setting the fastest gating variable equal to its steady state. however, the previous study for the excitable system cannot be applied since the system is not a 2D system. An extra step is needed to reduce the dimension of the system so that the previous step can applied in the analysis of the neuron model. A potential way to study the spiking behavior is since the τ_{us} is relatively slower than others, V_{us} can be considered a fixed constant while the dynamic behavior of other variables is investigated. Fig. 10 shows the bifurcation diagram of a system with V_s as its bifurcation parameter where $V_{us} = 0.09$. The $I_{app} = 0$ selected to ensure the system is in spiking mode according to [15]. The similarity of the curve with the excitable study emphasizes that a single excitable system is adequate to generate spiking behavior considering our choice of realization method. By setting the system in busting mode [15], the

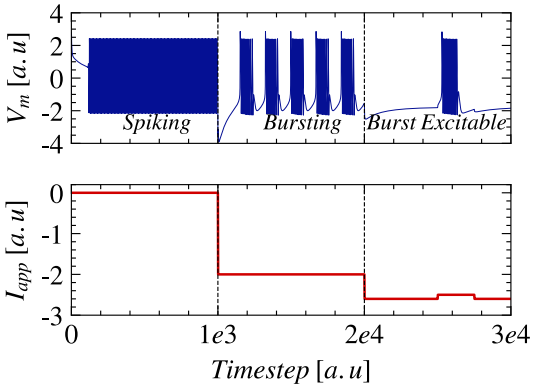

Fig. 12. Steady state behavior of the bio-mimetic neuron model for different modes of operation, modulated by external applied current, I_{app}.

same bifurcation analysis is done by assuming the V_{us} as the bifurcation parameter.

The blue traces are stable EQP, while the red traces denote unstable EQP. The orange traces are the projection of the oscillating trajectory in this system, corresponding to a spike and burst in Fig. 10 and Fig. 11 respectively. In Fig. 11 cyan trace denotes maximum and minimum V_m values along unstable periodic orbits and green traces denote maximum and minimum V_m values along stable periodic orbits. When we allow V_{us} to evolve slowly, it drifts towards more negative values while the remaining variables are near their resting values (lower part of burst solution, along blue curve in Fig. 11). When V_{us} is sufficiently negative, the system of other variables undergoes a saddle-node bifurcation and the trajectory jumps to the attracting branch of stable period orbits of that system. This leads to spiking behavior, and as this continues, the net drift of V_{us} is towards less negative values (to the right in Fig. 11). Finally, V_{us} reaches the value where the periodic orbits terminate in a homoclinic bifurcation (near $V_{us} = -1.7$), and the trajectory jumps back down to near the resting state for the other variables once again.

The bifurcation study of the system distinguishes the roles of different voltage terms (state variables) in producing the solutions observed in the steady-state response simulations and phase portrait. Fig. 12 shows the steady state response of the neuron model under different modes of operation: spiking, bursting and burst excitable, modulated by a single parameter: the external applied current, I_{app}. In simulation of Fig. 10, Fig. 11 and Fig. 12 the $-|\alpha_f^-| = |\alpha_s^+| = 2$, $-|\alpha_s^-| =$

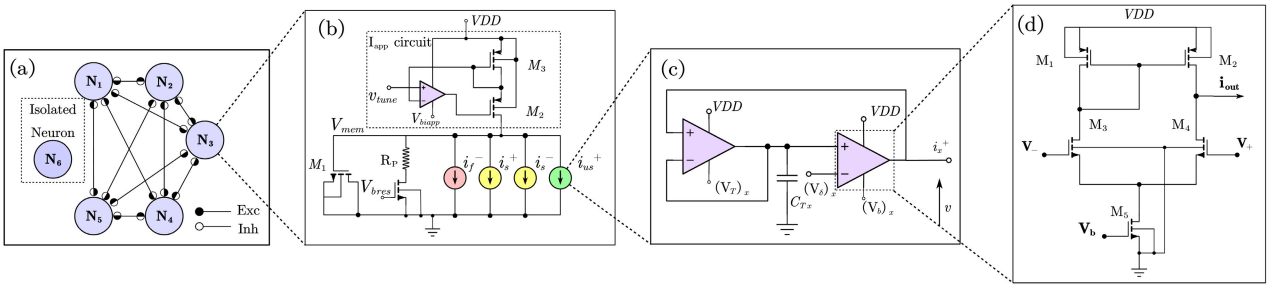

Fig. 13. Chip circuit diagram. (a) Network level diagram. 5 out of 6 neurons are fully connected with each other using tunable synapses. One isolated neuron is designed for I-V characteristic study. (b) Circuit diagram of a neuron. 4 parallel connected conductance channels and a passive RC circuit are included. The external current is controlled by 2 PMOS and an OTA. (c) Circuit diagram of conductance channel. The left OTA works as a tunable delay element and the right OTA provides the nonlinear transfer function. (d) Differential amplifier topology for Operational Transconductance Amplifier (OTA) used in synapse and neuron circuits. OTA consists of 5 MOSFETs. Output current i_{out} of the OTA is determined by the voltage V_b and the difference between V_+ and V_-.

$|\alpha_{us}^+| = 1.5$ and $|\delta_f^-| = |\delta_s^+| = 0$, $|\delta_s^-| = |\delta_{us}^+| = 0$ and ($\tau_f = 1$, $\tau_s = 50$, $\tau_{us} = 2500$).

IV. Hardware Implementation

This section describes how the neuron model, proposed in [15] and analyzed extensively in the previous section, is realized on silicon hardware with TSMC 180nm process technology. In addition to implementing single-neuron circuits, the test chip implements bio-mimetic neural networks interconnected with tunable synapses in order to test and validate network-level behavior.

A. BioNN Architecture

Fig. 13 shows the detailed architecture block diagram of the test chip. The chip consists of 2 bio-mimetic neural networks (BioNN) and each of them contains 6 neurons and 20 synapses. Within each neural network in the chip, 5 out of 6 neurons are fully interconnected to each other with two synapses between each pair of neurons and one isolated neuron for single neuron testing, as shown in Fig. 13(a). The circuit model of the individual neuron is shown in Fig. 13(b), as described in the background section. The membrane voltage outputs of the six neurons in each of the 4 networks are sent to voltage buffers that can drive large capacitive loads and enable accurate probing of the internal voltages. All neurons in the chip share common input bias voltages and bias currents, while the external stimulus current is set by two different voltages, vtune1 for the neurons N1, N2, N3 and vtune2 for the remaining 3 neurons N4, N5, and N6 of the 6-neuron network. For neuron network 1, the passive resistor R_p in each neuron is set to 1MΩ. For neuron network 2, R_p is set to 10MΩ, to provide a different range for passive current and explore the operating range of the neuron.

B. Circuit Design

Fig. 13(b) shows the circuit implementation of the neuron. 4 conductance channels are connected in parallel with a passive RC circuit. The 20pF membrane capacitor is replaced with M1 MIMCAP(Metal-Insulator-Semiconductor) with a small area. The 1MΩ and 10MΩ passive resistors are implemented with High-Resistance-Poly (HRP) material. A series NMOS transistor is connected to the passive resistor in order to limit the current I_p by tuning the gate voltage V_{bres}. In spiking

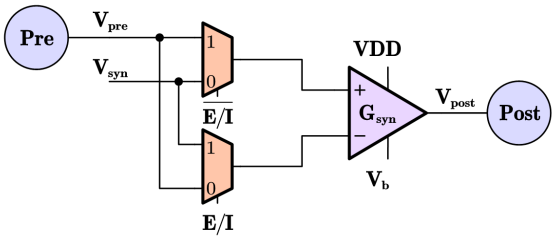

Fig. 14. Synapse circuit design. Membrane voltage of pre-neuron V_{pre} and bias voltage V_{syn} are connected to two 2-to-1 MUX, which decide the polarity of the synapse to be inhibitory or excitatory.

and bursting modes, the neuron membrane voltage has large excursions from 0V to 3.3V (VDD), and so will the current through the passive resistor swing from 0-3.3μA. Without the series connected NMOS gating, this current will affect the behavior of the neuron significantly, since the current needed to change behavior is only a few μA. The external current I_{app} is controlled by 2 series-connected PMOS and an operational transconductance amplifier (OTA), as shown in Fig. 13(b). The operating points of M_2 and M_3 are carefully set using the OTA-based feedback circuit such that the current through M_2 is decided by V_{tune}. In weak inversion region, the I-V relationship for M_2 can be described as $I_{DS} = I_0 e^{\frac{\kappa V_{GS}}{nV_T}}(1 - e^{\frac{-V_{DS}}{nV_T}})$ where $V_{DS} = V_{tune} - V_{mem}$ and $V_{GS} = V_{tune} - V_G$. The voltage drop of V_{GS} for M_2 could be treated as a constant value. So the current through M_2 and M_3 are simply decided by V_{tune} when the neuron is resting.

The circuit schematic of the negative conductance channel is shown in Fig. 13(c). It consists of 2 OTA and a latency capacitor. The circuit of the OTA, implemented using a simple differential amplifier topology, is shown in Fig. 14 (right). The simple circuit helps in reducing the area footprint of the neuron. It consists of 5 MOS transistors, two of which are PMOS and three are NMOS. The width and length of the PMOS M_1 and M_2 are 2.4μm and 1.6μm respectively. The NMOS M_5 has the same length and width as the PMOS. The differential pair NMOS transistors M_3 and M_4 are designed with 600nm width and 400nm length. The first OTA of the conductance channel acts as a voltage-follower with a delay that is tuned by the bias voltage, V_{Tx}. The second OTA provides the nonlinear transfer function, which can be the hyperbolic tangent function in the weak inversion region or can be a quadratic function if the transistor operates in strong inversion. The gain of the OTA, α is positive and set by

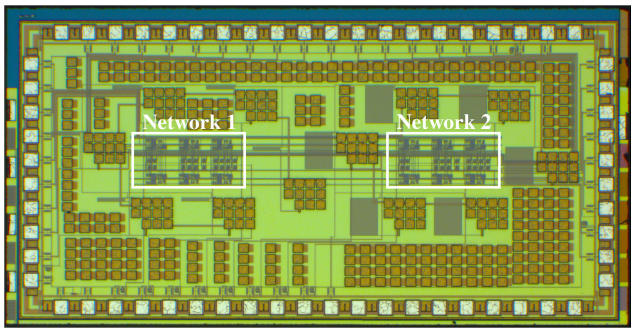

Fig. 15. Micrograph photo of the BioNN chip. Implemented in 180nm CMOS technology, the total chip area is 1mm x 2mm.

TABLE I
NEURON BIAS VOLTAGE PARAMETERS FOR ALL MODES

Conductance Channel vs Bias Voltage	Fast Negative	Slow Positive	Slow Negative	Ultra Slow Positive
V_δ (V)	0.75	0.55	0.55	0.45
V_τ (V)	1.75	1.75	1.48	1.48
V_b (V)	1	1.05	0.95	0.95

the bias voltage v_b where increasing v_b causes the amplitude of the transfer function to increase. The slope and offset of the transfer function can be tuned by bias voltages v_b and v_δ respectively. Positive and negative feedback of the dependent current source is obtained by flipping the positive and negative terminal of the second OTA.

Neurons are connected with tunable synapses which can be selected to be excitatory or inhibitory. The tunable synapse is designed with the same OTA implemented in the conductance channel, as shown in Fig. 14 (left). The membrane voltage of the pre-synaptic neuron and offset voltage V_{syn} are connected to the input terminals of the OTA. Two 2-to-1 multiplexers are used for polarity reversal and hence enabling an excitatory or inhibitory connection between the pre-synaptic neuron and post-synaptic neurons. When V_{pre} is connected to the positive input and V_{syn} is connected to the negative, the synapse inhibits the post-synaptic neuron. When the input terminals are reversed by switching the MUX select bit, the synapse excites the post-synaptic neuron. The voltage bias V_b tunes the transconductance gain of the OTA, G_{syn} which sets the synapse strength/weight.

V. MEASUREMENT RESULTS

Fig. 15 is the micrograph of the prototype BioNN chip fabricated on 180nm process technology. The supply voltage is 3.3V and the total chip area is 1mm x 2mm. The area occupied by a single neuron is 70μm x 37μm and the area occupied by a neural network (BioNN) of 6 neurons and 20 synapses is 0.32mm x 0.17mm. Table I provides the bias voltage parameters used for testing single neurons and neural networks implemented using the BioNN chip.

A. Single Neuron

One neuron in each network is isolated with no synapses or internal I_{app} generation circuit (transistors M_2, M_3 and the

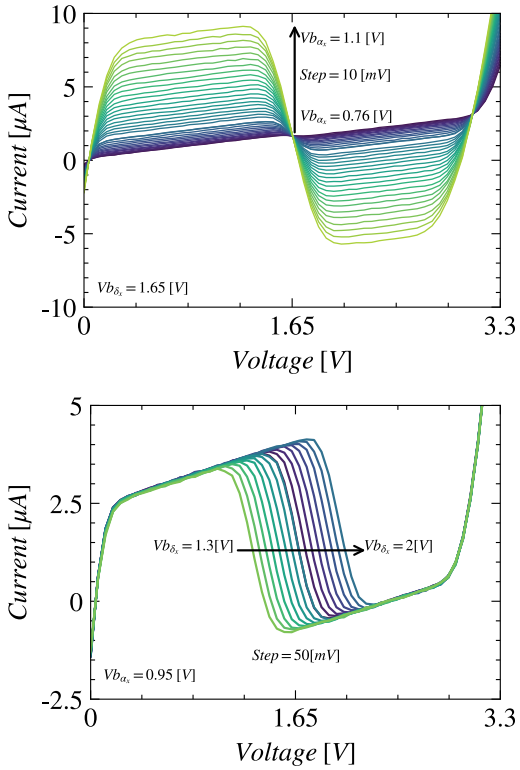

Fig. 16. On top, I-V curve for fast negative conductance channel when $V_{b\alpha}$ increases from 0.76V to 1.1V. Amplitude of the I-V curve increases accordingly. On the bottom, I-V curve for fast negative conductance channel when $V_{b\delta}$ changes. The center axis of the decreasing area of the I-V curve is shifting from left to right when $V_{b\delta}$ is increasing from 1.3V to 2V.

OTA using v_{tune} in Fig. 13 (b)) for single neuron characterization study. The I-V curve measurement of the isolated neuron will be used as the reference for tuning the dynamical behavior of the BioNN network. To generate I-V curve at different timescales, the isolated neuron circuit must parallelly connect a passive RC circuit with the relevant conductance channels. For the I-V curve at fast timescale, the fast negative conductance channel is chosen where the membrane voltage is swept from 0V to VDD (3.3V) and the current consumption is measured. When V_b increases from 0.76V to 1.1V, the amplitude of the I-V curve increases from 1μA to 9μA accordingly as shown in Fig. 16 (top). The larger current value provides a wider range for neurons to spike or burst, resulting in robust behavior. On the other hand, when V_δ is swept from 1.3V to 2V and other conditions remain the same, the central axis of the decreasing area in the I-V curve shifts accordingly, as shown in Fig.16 (bottom). Staggering the position of the fast conductance center axis and slow negative conductance center axis allows neurons to exhibit burst of spikes and resting periods alternatively.

The blue and red curves in Fig. 17 (left) are the bistable I-V curves for the fast and slow excitable circuits respectively. The black curve shows the overall I-V relationship when all 4 conductance channels in parallel (fast negative, slow positive, slow negative and ultraslow positive) are involved. As shown in Fig. 17 (left), when the voltage increases from 0 to 3.3V, the current changes accordingly and traces an "N" shape for both fast (blue) and slow (red) excitable circuits. This confirms the nonlinear operation of the combination of voltage

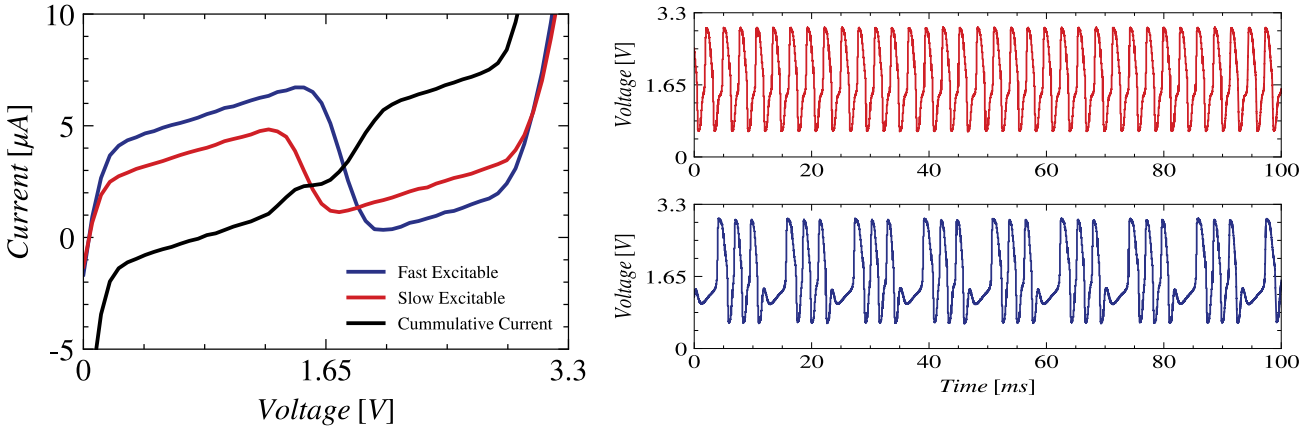

Fig. 17. Isolated neuron measurement results. On the left is the I-V characterization curve measured for different timescale conductance channels parallelly connected with passive RC circuit. Blue: Fast negative conductance channel. Red: Slow negative conductance channel. Black: Cumulative current for 4 conductance channels. On the right, is the neuron membrane voltage in spiking and bursting modes. (Top) Spiking mode with Iapp = 4μA. (Bottom) Bursting mode with Iapp = 2μA.

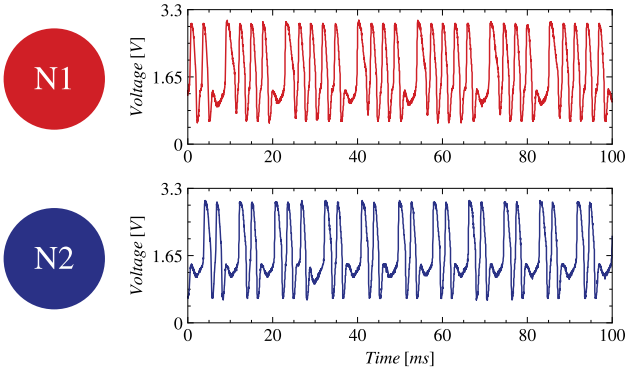

Fig. 18. Measured results of a neural network with two neurons, in bursting mode, without synapses (weak strength). The phase relationship between the two neurons bursting is arbitrary since there is no synaptic coupling.

dependent current sources $i_f{}^-$, $i_s{}^+$, $i_s{}^-$ and $i_{us}{}^+$ and enables the necessary bistability (local maxima and minima) condition required to generate limit cycles during bifurcation with I_{app}, as discussed in the previous section and also described in [15]. The overlap of the decreasing region, when voltage is around 1.4-1.8V, for both excitable circuits indicates the external current range needed to trigger bursting behavior. In this case, the burst range for external current is from 1μA to 4μA. When the external current is along the fast excitable decreasing region but out of the slow excitable decreasing region, the neuron exhibits spiking behavior. Quantitatively, when the external current I_{app} ranges between 4μA to 7μA, the single neuron will spike. Hence, it is possible to determine the range of externally applied current for the neuron to produce spiking and bursting behavior.

Fig. 17 (right) shows the isolated neuron membrane voltage waveform in spiking and bursting modes. When external current i_{app} is 4μA the neuron generates voltage spikes (red waveform) rising from 0.62V to 3V in 1.84ms. The average spike period or Inter Spike Interval (ISI) is 2.82ms resulting in a spike frequency of 357Hz. The blue waveform shows the bursting behavior of the neuron when i_{app} is 2μA, which is in the overlap area of the decreasing regions of the fast and slow I-V curves. There are 3 spikes for every burst and the average burst period is 7.68ms, leading to intraburst frequency of 391Hz. During bursting, the membrane voltage rises from 0.62V to 3V. The interburst period is 4.5ms and the resting voltage swing is within 0.2V.

B. Neural Network

The single isolated neuron characterization study with an external applied current provided the operating range for the spiking and bursting modes for the neuron. The next step is to setup different network topologies with the remaining 5 neurons in the network, interconnecting them with synapses that can be configured to provide excitatory or inhibitory synaptic currents, along with the tunable internal applied current. All possible configurations of a two neuron network are explored, where both neurons are tuned to burst and they have excitatory or inhibitory or no synaptic connections between them. Modulating the excitability of a neuron has a profound influence on the behavior not only at the neuron scale but also across scales [25]. This neuromodulatory behavior is best illustrated in two fundamental interconnection motifs that have been extensively studied in neuroscience: the I-I motif and the E-E motif. The I-I/E-E motif is a symmetric inhibitory/excitatory interconnection between two neurons, each controlling a network inhibitory/excitatory synaptic current into the other neuron.

Two neurons in the network are setup to burst with the interconnecting synapses disabled, as shown in Fig. 18. In this case, the bursting rhythms by the two neurons are uncorrelated since the synapse has minimum weight (negligible G_{syn}). For neuron N_1 (red curve), each burst includes 4 to 5 spikes, while neuron N_1 (blue) has 2 spikes per burst. In both neurons, the interburst period is set to 4.5ms. The different spikes per burst in the two neurons, even though all other parameters are the same, can be due to inherent random noise variation in a highly nonlinear system or possible device mismatch. When the two synapses between these two neurons are configured in excitatory mode, the membrane voltage of the two neurons is synchronized as shown in Fig. 19 (left), demonstrating the E-E motif found in neuroscience. Once synchronized to be "in-phase", it turns out that the number of spikes per burst approaches the average value of the 2 neurons, and hence

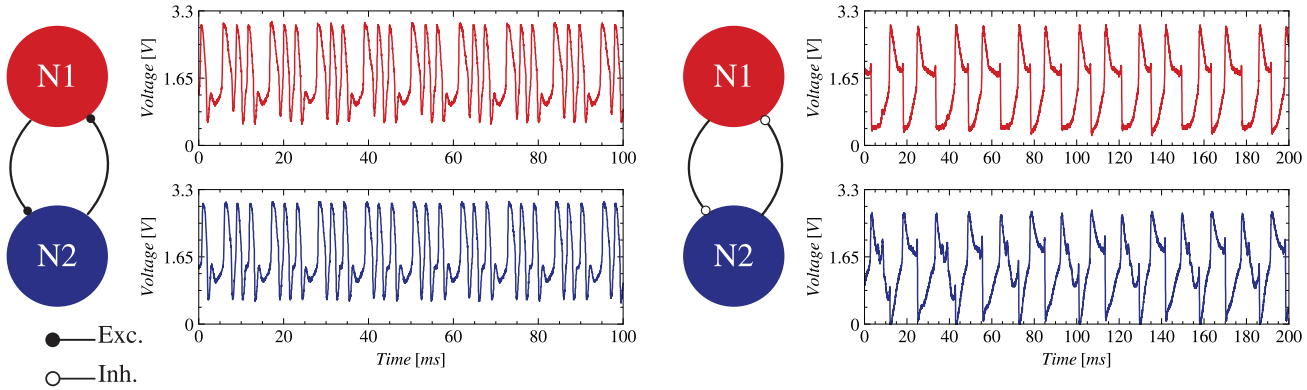

Fig. 19. Measured results of a neural network with two neurons in bursting mode with two excitatory synaptic connections (E-E motif on left) and two inhibitory synaptic connections (I-I motif on right). The phase of bursting is synchronized for the E-E motif where the number of spikes per burst is averaged out. For I-I motif, the neuron bursts/spikes are out of phase.

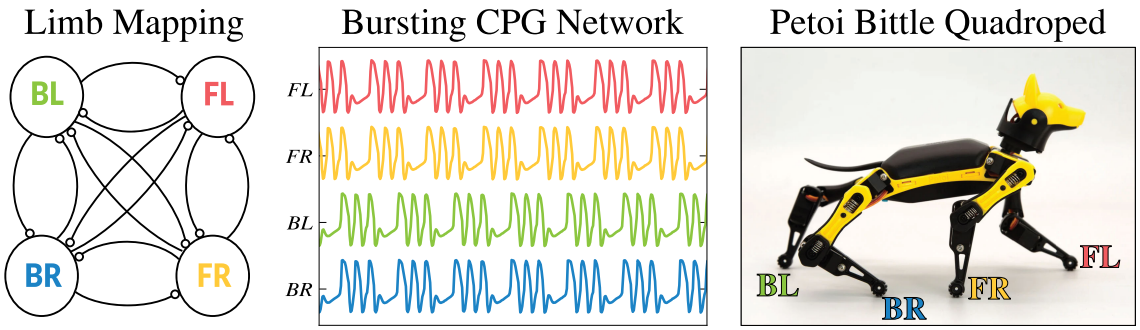

Fig. 20. CPG network to control the four legs of the Petoi Quadruped bot (left). Membrane voltage of the four neuron network implemented using BioNN chip to produce precise bursting rhythm for jump motion, with FL and FR in-phase with each other, as are BL and BR. The F pair is out-of-phase with the B pair (middle). Each neuron controls one leg of the robotic dog. Photo of the Petoi, a dog-like robot dog with the four limbs labeled (right).

3 spikes per burst can be evidently seen. The interburst period is the same as before the synapses were tuned.

Fig. 19 (right) shows the neuron membrane voltage when the synapse changes from excitatory to inhibitory mode, establishing the I-I motif. Here the expected result is that the two neurons produce "out-of-phase" synchronization in the bursting rhythms with the same number of spikes per burst. Though the measured results show the expected out-of-phase synchronization, the membrane voltage is barely bursting with almost 1-1.5 spikes per burst. This behaviour is possibly due to the timescale of the OTA-based synapse is much slower than the neuron spike, resulting in the reduction of spikes per burst. As shown in Fig. 19 (right), the intraburst period for both neurons is measured to be 10ms, and so is the interburst period. The spike amplitude of the neuron N_1 is 2.4V and the amplitude of neuron N_2 is 3V. The future work will focus on reducing the synaptic delay so that neurons can generate multiple spikes in the bursting phase.

C. Application - Robot Locomotion

The I-I motif is central to the circuit neurophysiology of CPG. To demonstrate an application with BioNN, a four neuron network is set up as a CPG network to control the motors of a quadruped (four legs) robot, Petoi Bittle, as shown in Fig. 20 (left). The four neurons can be divided into two pairs where two neurons controlling the front legs (front left: FL and front right: FR) make one pair, and the two neurons controlling the back legs (back left: BL and back right: BR) make another pair. With proper tuning using the same bias parameters discussed previously, the two pairs can be made to burst in-phase i.e. FL and FR form an E-E motif, BL and BR another E-E motif, whereas the pairs are out-of-phase with each other, i.e. FL and BL form an I-I motif, FR and BR form another I-I motif, as shown in Fig. 20 (middle). Because the network is connected all-to-all with inhibitory synapses, there is the potential for disinhibition to occur, in which the activation of one neuron causes a net decrease in the inhibition to one of the other neurons. This disinhibition can give rise to an effective excitatory, and indeed FL and FR behave equivalently to an E-E motif, as do BL and BR. Hence, by tuning the four neurons in this particular setting leads to a bursting rhythmic gait resulting in the robotic dog, Petoi, jumping in a periodic manner.

Our previous work demonstrated robot locomotion through bursting CPG rhythms programmed on the Arduino platform [17]. In this study, the membrane voltages from two E-E motif pairs were recorded from the BioNN chip and stored as the CPG network output for the front leg and back leg pairs. The stored voltage data was converted to spikes or events using a simple thresholding scheme on the Arduino platform present on the Petoi bot. The out-of-phase relationship between the two E-E motifs was achieved by inserting a phase delay. The Arduino board was programmed to send customized motor commands to the servo motors on each leg, for each spike in the bursting rhythm shown in Fig. 20 (right). The bursting rhythm provides fine-grain motor control resulting in a smoother movement of the legs, compared to spiking CPG rhythms in other work [32]. The video that recorded the jump behavior of the robot is available at youtu.be/7eQWEoVon9c.

TABLE II
ARCHITECTURE AND PERFORMANCE COMPARISON WITH STATE-OF-THE-ART BIOPHYSICAL NEURON IMPLEMENTATIONS

Publication	TBioCAS 2010 [33], TBioCAS 2017 [34]	Proc. of IEEE 2014 [5]	TCAD 2015 [4]	TVLSI 2016 [35], TBioCAS 2018 [36]	TBioCAS 2018 [37]	TBioCAS 2018 [38], TCAS-I 2018 [39]	Proc. of IEEE 2018 [40]	IEEE Micro 2018 [41]	TBioCAS 2019 [42]	TCAS-I 2023 [43]	This Work
Chip Name	NeuroDyn	SpiNNaker	TrueNorth	FPAA	DYNAPs	BrainScaleS	Braindrop	Loihi	ODIN	Zynq FPGA	BioNN
Implementation	Analog	Digital	Digital	Analog	Mixed-signal	Mixed-signal	Mixed-signal	Digital	Digital	Digital	Analog
CMOS Technology	500nm	130nm	28nm	350nm	180nm	65nm	28nm	14nm FinFET	28nm FDSOI	28nm	180nm
Supply Voltage (V)	5	1.2	0.7-1.05	3.3	1.3-1.8	2.5/1.2	1	0.5-1.25	0.55-1.0	1.0/1.8/3.3	3.3
Neuron Model	HH and extended ML	Program-mable	Augmented LIF**	Program-mable	Adaptive-Exponential LIF	Adaptive-Exponential LIF	Quadratic LIF	Program-mable	LIF and Izhikevich	Program-mable	Proposed Bio-mimetic
Area per Neuron (μm^2)	600000*	3745.3*	2900	215561*	29411*	2352	27.5	384.6*	333.3*	153(HH**), 125(IZ**), 144(ML**) Slices	2590
Power per Neuron (μW)	129*	NA	0.195*	0.79*	1500-3600	14.4	NA	NA	0.107 (0.55V)	128000(HH), 91000(IZ), 102000(ML)	907 (Spike), 1292 (Burst)
Energy per Spike (pJ)	774000*	26600	26	0.0135	260-883	620-960	0.380	23.6	12.7	329(HH), 132.6(IZ), 201.08(ML)	697000 (Spike), 969000 (Burst)

* The values indicated here are not explicitly mentioned in the provided reference(s); they are calculated based on the information provided in the article(s). Parameters for TrueNorth, DYNAPs, Loihi, SpiNNaker, ODIN were inferred/derived from Table I in [42]. Parameters for NeuroDyn, FPAA, BrainScaleS, Braindrop and Zync FPGA were inferred from the corresponding references.
** Neuron Models: HH - Hodgkin-Huxley, IZ - Izhikevich, ML - Morris Lecar, LIF - Leaky Integrate and Fire. NA - Not Available.

VI. DISCUSSION

Previous work on bio-inspired neuron models implemented on hardware such as the Hodgkin-Huxley, Morris-Lecar or Izhikevich neurons have non-intuitive equations and parameters, are computationally expensive and most importantly do not enable neuromodulatory control with a single parameter (I_{app}) at a network level to realize fundamental motifs in neuroscience such as the I-I motif. The bio-mimetic neuron model considered in this work is based on an intuitive control theory perspective comprising a mixed-feedback system (combination of positive and negative feedback currents) operating at multiple timescales (fast, slow, and ultraslow spanning μs to 100ms) [15]. This model is simultaneously bio-mimetic, by mimicking the Na+/K+ channel activation and deactivation mechanisms found in neurophysiology, while being hardware-friendly, with implementation using simple analog delay elements and OTA-based nonlinear activation function (tanh or quadratic). For the first time, to the best of our knowledge, this work shows the hardware realization of the bio-mimetic neuron model that can be used to form neural networks (BioNN) to generate tightly coupled rhythms using neuromodulatory control.

Before implementing the bio-mimetic neuron model on hardware, we found it imperative to understand the inner workings of the fast and slow excitable systems in the neuron by modeling them as a 4-dimensional nonlinear dynamical system and performing extensive bifurcation analysis. The analysis helped in understanding the excitability of the neuron under different conditions and how the parameters of the individual conductance channels, such as gain, offset and delay of the nonlinear activation function, operating at fast, slow, and ultraslow timescales affect the membrane voltage dynamics including the mode of operation (spiking or bursting), voltage amplitude and spiking or bursting (intraburst and interburst) frequency. The results from the analysis proved it is not possible to get bursting behavior with only one of these excitable systems. Two excitable systems operating at sufficiently separated timescales with mixed-feedback were essential to achieve complex bursting dynamics through careful tuning of the parameters and understanding the phase portraits obtained through different bifurcation studies. Hence the mathematical analysis helped in informing how to tune the neuron model in hardware to operate in different regimes (spiking, bursting) by characterizing the fast and slow sub-systems and determining the tunable range of external input current.

The custom BioNN ASIC is implemented with 180nm CMOS technology and the overall power consumption of the chip, with 12 neurons and 40 synapses, is 10.88mW on average. Table II summarizes the results of this work compared to the state-of-the-art. The energy needed to generate a spike for the BioNN chip is 697nJ, which is calculated (for spiking or bursting mode) by Power x N_{spikes} x Time. Though the power consumption and area footprint of the BioNN is comparable but larger than the state-of-the-art analog or mixed-signal neurons, we intended this work to primarily serve as a proof of concept to demonstrate the proposed BioNN neurons and networks that can generate tunable bursting rhythms through neuromodulatory control. As future work, we plan to scale the BioNN aggressively to a deep-submicron technology to optimize for area and energy efficiency, allowing scalability

to build larger networks. We also plan to consider emerging beyond-CMOS devices to replace the OTA based elements in the neuron model to generate delay at multiple timescales and enable nonlinear activation function for the parallel conductance channels.

VII. Conclusion

This paper presents a mathematical analysis and hardware realization of bio-mimetic neural networks (BioNN) using a nonlinear neuron model that utilizes two excitable systems, designed from a control theory perspective. The neuron is modeled as a mixed-feedback system operating at multiple timescales that can be tuned to produce spiking and bursting behavior. A comprehensive understanding of the system's dynamic behavior was successfully obtained by studying the state variables space and performing bifurcation analysis on the different parameters that constitute the autonomous system of ordinary differential equations (ODEs) governing the neuron model. The bifurcation study of the neuron model as a 4D dynamical system described the expected phase trajectories of the membrane voltage.

The proposed BioNN was implemented on a prototype chip utilizing the 180nm CMOS process technology. This chip implements two neural networks, each containing a different passive resistor. Each neural network consists of 1 isolated neuron, 5 fully connected neurons, and 20 synapses. The behavior of these neurons is related to the I-V curve of diverse time-scale excitable circuits. By carefully selecting bias voltages, the neuron could seamlessly shift between spike, burst, and burst excitable behavior.

The neurons can exhibit rhythmic patterns found in tightly coupled neural networks in biology, such as the CPGs, allowing neuromodulatory control on hardware at nodal and network levels. Recreating the CPG, crucial for movement in animals, can enable robust sensorimotor control for robotic locomotion. To demonstrate the use of BioNN in a real-world application, the generated burst waveforms from the BioNN chip are applied to a CPG, allowing it to control a robotic dog to execute a jumping motion. It is possible to scale the size and power of the neuron further by porting to a deep-submicron technology node, thereby enabling large-scale neuromorphic neural networks with nonlinear dynamics inspired by biology.

Acknowledgment

The authors would like to thank Prof. Feng Xiong, University of Pittsburgh, for his input on hardware testing and network characterization plots. They would also like to thank graduate student Vijay Shankaran Vivekanand for his help in programming the Petoi robot for the BioNN application.

References

[1] O. I. Abiodun, A. Jantan, A. E. Omolara, K. V. Dada, N. A. Mohamed, and H. Arshad, "State-of-the-art in artificial neural network applications: A survey," *Heliyon*, vol. 4, no. 11, Nov. 2018, Art. no. e00938.

[2] B. G. Buchanan, "A (very) brief history of artificial intelligence," *AI Mag.*, vol. 26, no. 4, p. 53, Dec. 2005.

[3] T. Szandała, "Review and comparison of commonly used activation functions for deep neural networks," in *Bio-Inspired Neurocomputing*. Cham, Switzerland: Springer, 2021, pp. 203–224.

[4] F. Akopyan et al., "TrueNorth: Design and tool flow of a 65 mW 1 million neuron programmable neurosynaptic chip," *IEEE Trans. Comput.-Aided Design Integr. Circuits Syst.*, vol. 34, no. 10, pp. 1537–1557, Oct. 2015.

[5] S. B. Furber, F. Galluppi, S. Temple, and L. A. Plana, "The SpiNNaker project," *Proc. IEEE*, vol. 102, no. 5, pp. 652–665, May 2014.

[6] L. F. Abbott, "Lapicque's introduction of the integrate-and-fire model neuron (1907)," *Brain Res. Bull.*, vol. 50, nos. 5–6, pp. 303–304, Nov. 1999.

[7] W. Maass, "Networks of spiking neurons: The third generation of neural network models," *Neural Netw.*, vol. 10, no. 9, pp. 1659–1671, Dec. 1997.

[8] X. Yao, F. Li, Z. Mo, and J. Cheng, "GLIF: A unified gated leaky integrate-and-fire neuron for spiking neural networks," in *Advances in Neural Information Processing Systems*, vol. 35, S. Koyejo, S. Mohamed, A. Agarwal, D. Belgrave, K. Cho, and A. Oh, Eds. Red Hook, NY, USA: Curran Associates, Inc., 2022, pp. 32160–32171. [Online]. Available: https://proceedings.neurips.cc/paper_files/paper/2022/file/cfa8440d500a6a6867157dfd4eaff66e-Paper-Conference.pdf

[9] D. Chatterjee and A. Kottantharayil, "A CMOS compatible bulk FinFET-based ultra low energy leaky integrate and fire neuron for spiking neural networks," *IEEE Electron Device Lett.*, vol. 40, no. 8, pp. 1301–1304, Aug. 2019.

[10] L. Ribar and R. Sepulchre, "Bursting through interconnection of excitable circuits," in *Proc. IEEE Biomed. Circuits Syst. Conf. (BioCAS)*, Oct. 2017, pp. 1–4.

[11] E. M. Izhikevich, "Which model to use for cortical spiking neurons?" *IEEE Trans. Neural Netw.*, vol. 15, no. 5, pp. 1063–1070, Sep. 2004.

[12] E. Marder, "Neuromodulation of neuronal circuits: Back to the future," *Neuron*, vol. 76, no. 1, pp. 1–11, Oct. 2012.

[13] A. Hodgkin and A. Huxley, "A quantitative description of membrane current and its application to conduction and excitation in nerve," *Bull. Math. Biol.*, vol. 52, nos. 1–2, pp. 25–71, 1990.

[14] E. M. Izhikevich, "Simple model of spiking neurons," *IEEE Trans. Neural Netw.*, vol. 14, no. 6, pp. 1569–1572, Nov. 2003.

[15] L. Ribar and R. Sepulchre, "Neuromodulation of neuromorphic circuits," *IEEE Trans. Circuits Syst. I, Reg. Papers*, vol. 66, no. 8, pp. 3028–3040, Aug. 2019.

[16] P. A. Guertin, "The mammalian central pattern generator for locomotion," *Brain Res. Rev.*, vol. 62, no. 1, pp. 45–56, Dec. 2009.

[17] V. S. Vivekanand, S. Chopra, S. Hashemkhani, and R. C. Kubendran, "Robot locomotion through tunable bursting rhythms using efficient biomimetic neural networks on Loihi and Arduino platforms," in *Proc. Int. Conf. Neuromorphic Syst.*, Aug. 2023, pp. 1–7.

[18] K. Nakada, T. Asai, and Y. Amemiya, "An analog CMOS central pattern generator for interlimb coordination in quadruped locomotion," *IEEE Trans. Neural Netw.*, vol. 14, no. 5, pp. 1356–1365, Sep. 2003.

[19] K. Nakada, T. Asai, T. Hirose, and Y. Amemiya, "Analog CMOS implementation of a neuromorphic oscillator with current-mode low-pass filters," in *Proc. IEEE Int. Symp. Circuits Syst.*, Kobe, Japan: May 2005, pp. 1923–1926. [Online]. Available: http://ieeexplore.ieee.org/document/1464989/

[20] M. F. Simoni, G. S. Cymbalyuk, M. E. Sorensen, R. L. Calabrese, and S. P. DeWeerth, "A multiconductance silicon neuron with biologically matched dynamics," *IEEE Trans. Biomed. Eng.*, vol. 51, no. 2, pp. 342–354, Feb. 2004. [Online]. Available: http://ieeexplore.ieee.org/document/1262112/

[21] P. Arena, L. Fortuna, M. Frasca, L. Patane, and G. Vagliasindi, "CPG-MTA implementation for locomotion control," in *Proc. IEEE Int. Symp. Circuits Syst.*, Kobe, Japan, Mar. 2005, pp. 4102–4105. [Online]. Available: https://ieeexplore.ieee.org/document/1465533

[22] R. J. Kier, J. C. Ames, R. D. Beer, and R. R. Harrison, "Design and implementation of multipattern generators in analog VLSI," *IEEE Trans. Neural Netw.*, vol. 17, no. 4, pp. 1025–1038, Jul. 2006. [Online]. Available: http://ieeexplore.ieee.org/document/1650256/

[23] F. Tenore, R. Etienne-Cummings, and M. A. Lewis, "A programmable array of silicon neurons for the control of legged locomotion," in *Proc. IEEE Int. Symp. Circuits Syst.*, Vancouver, BC, Canada, Feb. 2004. [Online]. Available: http://ieeexplore.ieee.org/document/1329534/

[24] E. M. Izhikevich, *Dynamical Systems in Neuroscience*. Cambridge, MA, USA: MIT Press, 2007.

[25] R. Sepulchre, G. Drion, and A. Franci, "Control across scales by positive and negative feedback," *Annu. Rev. Control, Robot., Auto. Syst.*, vol. 2, no. 1, pp. 89–113, May 2019.

[26] K. Liu, S. Hashemkhani, J. Rubin, and R. Kubendran, "Neuromorphic networks using nonlinear mixed-feedback multi-timescale bio-mimetic neurons," in *Proc. IEEE Int. Symp. Circuits Syst. (ISCAS)*, May 2023, pp. 1–5.
[27] E. M. Izhikevich, *Dynamical Systems in Neuroscience: The Geometry of Excitability and Bursting*. Cambridge, MA, USA: MIT Press, 2006. [Online]. Available: https://direct.mit.edu/books/book/2589/dynamical-systems-in-neurosciencethe-geometry-of
[28] R. Sepulchre, G. Drion, and A. Franci, "Excitable behaviors," in *Emerging Applications of Control and Systems Theory: A Festschrift in Honor of Mathukumalli Vidyasagar*. Cham, Switzerland: Springer, 2018, pp. 269–280.
[29] J. C. Willems, "The behavioral approach to open and interconnected systems," *IEEE Control Syst.*, vol. 27, no. 6, pp. 46–99, Dec. 2007.
[30] E. M. Izhikevich, "Neural excitability, spiking and bursting," *Int. J. Bifurcation Chaos*, vol. 10, no. 6, pp. 1171–1266, Jun. 2000.
[31] L. Perko, *Differential Equations and Dynamical Systems*, vol. 7. Cham, Switzerland: Springer, 2013.
[32] A. S. Lele, Y. Fang, J. Ting, and A. Raychowdhury, "Learning to walk: Spike based reinforcement learning for hexapod robot central pattern generation," in *Proc. 2nd IEEE Int. Conf. Artif. Intell. Circuits Syst. (AICAS)*, Aug. 2020, pp. 208–212.
[33] J. Wang, D. Breen, A. Akinin, F. Broccard, H. D. I. Abarbanel, and G. Cauwenberghs, "Assimilation of biophysical neuronal dynamics in neuromorphic VLSI," *IEEE Trans. Biomed. Circuits Syst.*, vol. 11, no. 6, pp. 1258–1270, Dec. 2017.
[34] T. Yu and G. Cauwenberghs, "Analog VLSI biophysical neurons and synapses with programmable membrane channel kinetics," *IEEE Trans. Biomed. Circuits Syst.*, vol. 4, no. 3, pp. 139–148, Jun. 2010.
[35] S. George et al., "A programmable and configurable mixed-mode FPAA SoC," *IEEE Trans. Very Large Scale Integr. (VLSI) Syst.*, vol. 24, no. 6, pp. 2253–2261, Jun. 2016.
[36] A. Natarajan and J. Hasler, "Hodgkin–Huxley neuron and FPAA dynamics," *IEEE Trans. Biomed. Circuits Syst.*, vol. 12, no. 4, pp. 918–926, Aug. 2018.
[37] S. Moradi, N. Qiao, F. Stefanini, and G. Indiveri, "A scalable multicore architecture with heterogeneous memory structures for dynamic neuromorphic asynchronous processors (DYNAPs)," *IEEE Trans. Biomed. Circuits Syst.*, vol. 12, no. 1, pp. 106–122, Feb. 2018.
[38] S. A. Aamir et al., "A mixed-signal structured AdEx neuron for accelerated neuromorphic cores," *IEEE Trans. Biomed. Circuits Syst.*, vol. 12, no. 5, pp. 1027–1037, Oct. 2018.
[39] S. A. Aamir et al., "An accelerated LIF neuronal network array for a large-scale mixed-signal neuromorphic architecture," *IEEE Trans. Circuits Syst. I, Reg. Papers*, vol. 65, no. 12, pp. 4299–4312, Dec. 2018.
[40] A. Neckar et al., "BrainDrop: A mixed-signal neuromorphic architecture with a dynamical systems-based programming model," *Proc. IEEE*, vol. 107, no. 1, pp. 144–164, Jan. 2019.
[41] M. Davies et al., "Loihi: A neuromorphic manycore processor with on-chip learning," *IEEE Micro*, vol. 38, no. 1, pp. 82–99, Jan. 2018.
[42] C. Frenkel, M. Lefebvre, J.-D. Legat, and D. Bol, "A 0.086-mm^2 12.7-pJ/SOP 64k-synapse 256-neuron online-learning digital spiking neuromorphic processor in 28-nm CMOS," *IEEE Trans. Biomed. Circuits Syst.*, vol. 13, no. 1, pp. 145–158, Feb. 2019.
[43] M. Ghanbarpour, A. Naderi, B. Ghanbari, S. Haghiri, and A. Ahmadi, "Digital hardware implementation of Morris–Lecar, Izhikevich, and Hodgkin–Huxley neuron models with high accuracy and low resources," *IEEE Trans. Circuits Syst. I, Reg. Papers*, vol. 70, no. 11, pp. 4447–4455, Nov. 2023.

Kangni Liu (Student Member, IEEE) received the B.S. degree in automation from the Beijing Institute of Technology, Beijing, China, in 2019, and the M.S. degree in electrical and electronic engineering from the University of Pittsburgh, Pittsburgh, PA, USA, in 2020, where she is currently pursuing the Ph.D. degree in electrical and electronic engineering. Her research interests include neuromorphic computing, biomedical instrumentation, and analog circuit design.

Shahin Hashemkhani (Student Member, IEEE) received the M.Sc. degree from Politecnico di Milano, with a focus on the characterization of emerging resistive switching memory (PCM and RRAM) and designing and implementing a neuromorphic system to take advantage of the novel device. He is currently pursuing the Ph.D. degree in electrical and computer engineering (ECE) with the University of Pittsburgh. His dissertation was focused on solving the constraints satisfaction problem with the spiking Hopfield networks, where the sudoku problem was solved on hardware for the first time. He is working with Prof. Xiong and Prof. Kubendran, at the University of Pittsburgh to continue studying the novel bio-inspired device and design chips to achieve more bio-realistic neural networks. He is deeply passionate about emerging electronic devices and new architecture that may lead to more efficient electronic products.

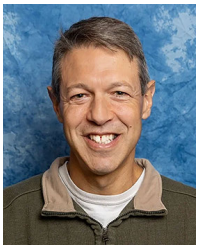

Jonathan Rubin (Member, IEEE) received the bachelor's degree in mathematics from the College of William and Mary and the Ph.D. degree in applied mathematics from Brown University in 1996. Before joining the Department of Mathematics, University of Pittsburgh, in 2000, he was a Zassenhaus Assistant Professor and then a National Science Foundation Post-Doctoral Fellow with the Department of Mathematics, The Ohio State University. He is currently a Professor of mathematics with the University of Pittsburgh. He is also a Graduate Faculty Member with the Center for Neuroscience, University of Pittsburgh; a Graduate Training Faculty Member with the Center for the Basis of Neural Cognition, McGowan Institute for Regenerative Medicine; a member of the SIAM Fellows Class of 2021; and a Visiting Professor in computational biology. He supervised or co-supervised 14 students to complete their Ph.D. studies. He has also mentored eight post-doctoral fellows.

Rajkumar Kubendran (Senior Member, IEEE) received the M.S. degree in electrical and computer engineering from Purdue University in 2012 and the Ph.D. degree from the University of California San Diego, with a focus on energy-efficient neuromorphic VLSI computing systems, spanning from devices to applications. He is currently an Assistant Professor with the Department of Electrical and Computer Engineering, University of Pittsburgh. He has demonstrated prototypes of dynamic vision sensors (DVS) and in-memory computing architectures with some of the best energy-efficiency metrics reported in the literature. He has interned with multiple analog and RF design teams in the industry, such as Intel, IMEC Belgium, MaxLinear, and Qualcomm. His research interests include low-power analog and mixed signal circuit design with emerging non-volatile memory devices to build event-driven architectures for computer vision and machine learning applications.